Developmental Cell
Article

The Apoptotic Regulator Nrz Controls Cytoskeletal Dynamics via the Regulation of Ca^{2+} Trafficking in the Zebrafish Blastula

Nikolay Popgeorgiev,[1,2] Benjamin Bonneau,[1,2] Karine F. Ferri,[2] Julien Prudent,[1,2] Julien Thibaut,[2] and Germain Gillet[1,2,*]
[1]CRCL U1052 INSERM, UMS 3443 CNRS, Centre Léon Bérard, 28 rue Laennec, 69008 Lyon, France
[2]IBCP UMR 5086 CNRS-Université Lyon I, IFR 128, 7, passage du Vercors, 69367 Lyon 07, France
*Correspondence: gillet@lyon.fnclcc.fr
DOI 10.1016/j.devcel.2011.03.016

SUMMARY

Bcl-2 family members are key regulators of apoptosis. Their involvement in other cellular processes has been so far overlooked. We have studied the role of the Bcl-2 homolog Nrz in the developing zebrafish. Nrz was found to be localized to the yolk syncytial layer, a region containing numerous mitochondria and ER membranes. Nrz knockdown resulted in developmental arrest before gastrulation, due to free Ca^{2+} increase in the yolk cell, activating myosin light chain kinase, which led to premature contraction of actin-myosin cables in the margin and separation of the blastomeres from the yolk cell. In the yolk syncytial layer, Nrz appears to prevent the release of Ca^{2+} from the endoplasmic reticulum by directly interacting with the IP3R1 Ca^{2+} channel. Thus, the Bcl-2 family may participate in early development, not only by controlling apoptosis but also by acting on cytoskeletal dynamics and cell movements via Ca^{2+} fluxes inside the embryo.

INTRODUCTION

The Bcl-2 family plays a central role in apoptosis; it controls the release of cytochrome *c* from the mitochondria into the cytosol, which triggers the formation of the apoptosome complex and caspase activation, leading to cell death. Cytochrome *c* release is due to the insertion of the apoptosis accelerator Bax into the outer mitochondrial membrane, which is blocked by Bcl-2 and related apoptosis inhibitors (for review, see Wang and Youle, 2009). In addition to the mitochondria, apoptosis inhibitors are also found in the endoplasmic reticulum (ER) where they participate in the regulation of Ca^{2+} fluxes (for review, see Rong and Distelhorst, 2008). Indeed, Bcl-2 modulates the release of Ca^{2+} from the ER by directly inactivating Bax and/or by interacting with the Ca^{2+} channel IP3R (Chen et al., 2004; Rong et al., 2009).

In addition to IP3R, Bcl-2 family members interact with a variety of partners, including G proteins (Bivona et al., 2006), phosphatases (Shibasaki et al., 1997), kinases (Wang et al., 1994; Youn et al., 2005), transcription factors (de Moissac et al., 1998), and chaperone proteins (Takayama et al., 1995; Shirane and Nakayama, 2003). This illustrates that Bcl-2 proteins play multiple roles inside the cell and can control the cell cycle (Zinkel et al., 2006), cell differentiation (Wang et al., 2007), axonal elongation (Jiao et al., 2005), redox status (Kowaltowski and Fiskum, 2005), and metabolism (Chen and Pervaiz, 2010). However, the underlying molecular mechanisms remain largely unknown.

The role of Bcl-2 like proteins during development was established by the work of R. Horwitz and M. Hengartner in *C. elegans* (Hengartner and Horvitz, 1994). Investigations in *Drosophila* and vertebrate models confirmed the role of the apoptosis machinery in development and morphogenesis (for review, see Chipuk et al., 2010).

The zebrafish is a unique model for studying the mechanisms of development in vertebrates (Shestopalov and Chen, 2010) and of a number of human pathologies, including cardiovascular diseases and cancer (Lam et al., 2006; Lieschke and Currie, 2007). During early development, after rapid cellular divisions, the blastomeres in contact with the yolk release their content in the yolk cell forming the yolk syncytial layer (YSL). At this stage the embryo comprises the YSL, the enveloping layer (EVL), and the deep cell layer (DCL). Prior to gastrulation, the blastomeres begin to migrate from the animal pole down to the vegetal pole. This process, known as epiboly, is driven by multiple mechanisms, including yolk cytoskeleton remodeling and endocytosis. Completion of epiboly is characterized by the formation of an actin-myosin ring close to vegetal pole of EVL and DCL (Solnica-Krezel, 2006).

We recently demonstrated that the knockdown of the apoptosis inhibitor *nrz* (the zebrafish ortholog of human *nrh/bcl-2l10*) leads to premature death of the embryo due to developmental arrest before the onset of gastrulation. This phenotype could be partly prevented by the downregulation of the Snail pathway, but not by caspase inhibition, suggesting that the effect of *nrz* knockdown might not be due to apoptosis deregulation (Arnaud et al., 2006).

Here, we show that *nrz* knockdown results in Ca^{2+}-dependent phosphorylation of the myosin light chain (MLC). We show that the knockdown of *nrz* increases free Ca^{2+} levels in the region of the margin (between the embryonic blastomeres and the yolk cell). We present evidence that the Ca^{2+}-dependent kinase MLCK is required for the observed MLC phosphorylation and subsequent epiboly arrest. Together, our results support the notion that the Nrz protein plays a key role during epiboly by controlling the formation of actin-myosin cables and cell movements via the regulation of Ca^{2+} fluxes from the ER. Thus, in

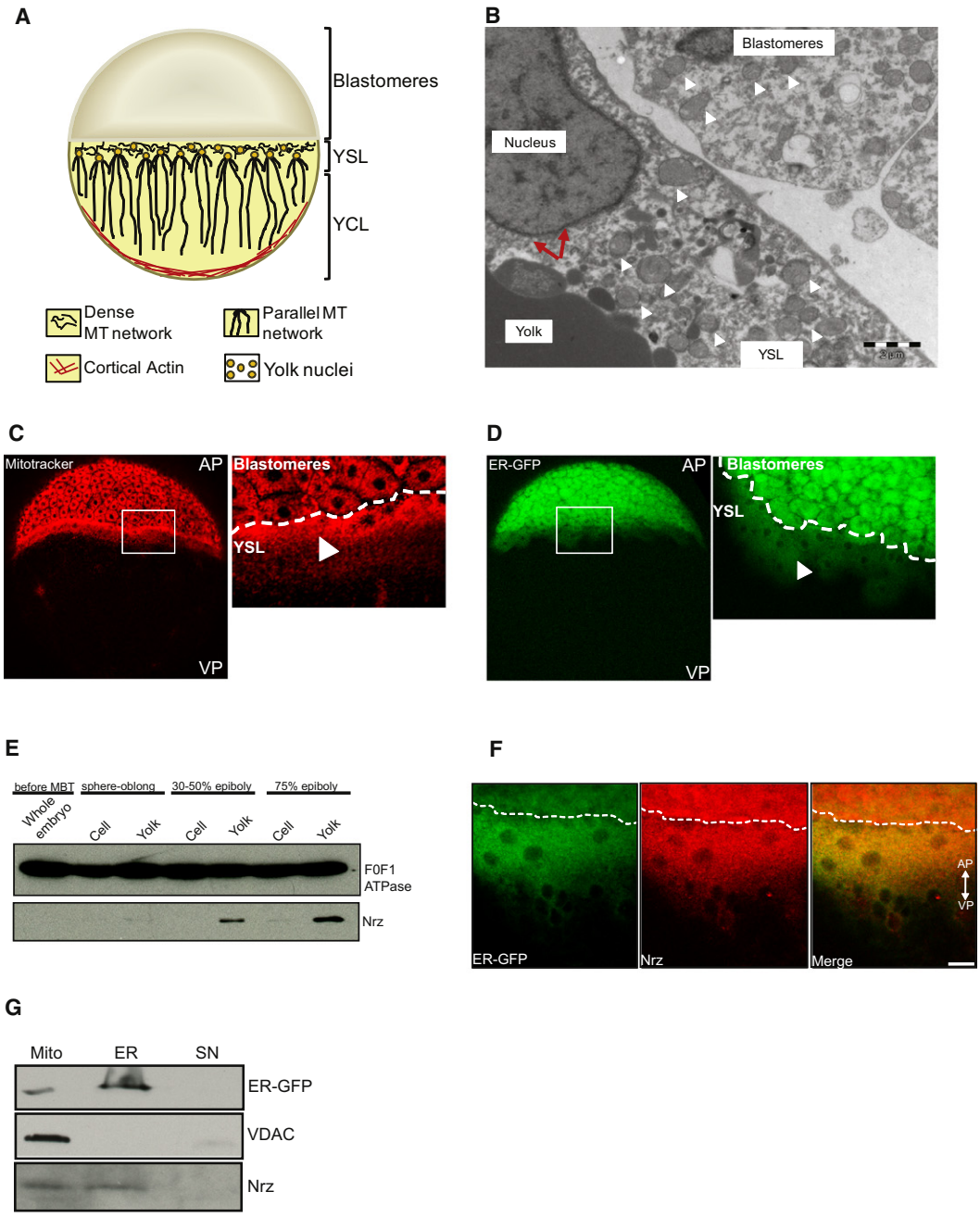

Figure 1. Nrz Protein Is Located into YSL Mitochondria and ER

(A) Schematic drawing of a zebrafish embryo representing a simplified model of yolk organization. YSL contains a large number of nuclei present beneath the blastoderm. The region populated with yolk nuclei presents a dense network of microtubules from which originates a parallel microtubule network oriented along the animal-vegetal axis and extending into the yolk cell layer. MT, microtubules; YSL, yolk syncytial layer; YCL, yolk cell layer.

(B) Transmission electron microscopy image of the interface region between the YSL and the deep cells showing the presence of numerous mitochondria inside the blastomeres and the YSL (white arrowheads). Membranes reminiscent from ER are visible in the vicinity of a YSL nucleus (red arrows). Scale bar: 2 μm.

(C) Confocal section of zebrafish embryo stained in vivo with Mitotracker Red in the margin region showing the presence of a belt of mitochondria in the YSL (arrowhead).

(D) Confocal section of zebrafish embryo expressing recombinant EGFP targeted into the ER membrane (ER-GFP); a fluorescent signal can be detected in the YSL (arrowhead). White rectangles materialize regions observed at higher magnification (right panels). AP, animal pole; VP, vegetal pole.

(E) Immunoblot of whole embryo (before MBT stage) or blastomere and yolk mitochondrial extracts (sphere-oblong, 30%–50%, or 75% epiboly stages) showing the presence of Nrz protein in the yolk mitochondrial fraction. F0/F1 ATPase is used for calibration.

(F) Confocal microscopy analysis. Detection of ER-GFP (green, left) and endogenous Nrz protein (red, middle) at the margin (50% epiboly). Merged images show colocalization of ER-GFP and Nrz (yellow, right). Dashed line separates blastomeres from YSL. Scale bar: 20 μm. Specificity of the anti-Nrz antibody was assessed using Nrz-depleted embryos as negative control (see Figure S1).

addition to controlling apoptosis, the Bcl-2 family may participate in the development of vertebrates by acting on cytoskeletal dynamics and cell movements.

RESULTS

Zebrafish YSL Harbors Active Mitochondria and ER Network

We previously showed that the *nrz* gene, a member of the *bcl-2* family of cell death regulators, is specifically expressed at the onset of epiboly in the extramaternal YSL of the zebrafish embryo (Arnaud et al., 2006). This belt-like layer contains a number of nuclei as well as microtubules, which participate in epiboly progression (Figure 1A) (Solnica-Krezel, 2006). In addition, the YSL is expected to contain a variety of components such as ER or Golgi apparatus, originating from the blastomeres having fused with the yolk cell. So far, the presence of mitochondria in the yolk cell of the developing zebrafish has not been reported. As shown in Figure 1B, transmission electronic microscopy analysis showed the presence of a number of mitochondria in the YSL. Protrusive structures originating from the nuclear envelope strongly suggested the existence of ER in this region. To further assess the presence of mitochondria and ER in the YSL, embryos were stained in vivo with the mitochondrial probe Mitotracker or injected with in vitro synthesized mRNAs encoding an EGFP mutant containing the transmembrane (TM) domain of the tail-anchored ER protein Cytochrome B5 (ER-GFP). Confocal microscopy analyses confirmed the presence of numerous mitochondria forming a ring like structure and of a dense ER network inside the YSL (Figures 1C, 1D, and S1A). Of note, the fact that YSL mitochondria could be labeled with Mitotracker, which is driven into the matrix by the mitochondrial transmembrane potential ($\Delta\Psi_m$), suggested that these organelles are actually functional.

In cultured cells, the Nrz protein is located in mitochondria and the ER (Figure S2A), which suggested that Nrz might also interact with these organelles in the YSL. Indeed, as shown in Figures 1E and S1B, the Nrz protein is detected in the YSL as early as the sphere-oblong stage both in mitochondria and ER fractions, remaining undetectable in the blastomeres. Confocal microscopy analyses and fractionation experiments confirmed the dual localization of Nrz in the YSL ER and mitochondria during epiboly progression (Figures 1F, 1G, S1B, and S1C).

Functional Interaction of Nrz with Mitochondria and ER Membranes into the YSL

Knockdown of *nrz* with specific morpholinos results in early developmental arrest (Arnaud et al., 2006); in *nrz* morphants, progression of the blastomeres down to the vegetal pole starts normally; however, this movement is stopped short before the margin reaches the equator of the yolk cell (40%–60% epiboly); premature constriction of the margin occurs at the same time, leading to separation of the blastomeres from the yolk and death of the embryo (Movie S1). Constriction of the margin was quantified by measuring the embryo length/width ratio (LWR) at 50% epiboly-shield stages. The LWR of control embryos is close to 1 (LWR = 1.001 ± 0.02, n = 34) whereas in *nrz* morphants it is significantly higher (LWR = 1.36 ± 0.06, n = 34) (Figures 2A and 2B).

The Bcl-2 family of proteins participates in the regulation of apoptosis and other cellular processes via interaction of their TM domain with mitochondrial and ER membranes (Rizzuto et al., 2009). Nrz contains a C-terminal TM domain, as do most Bcl-2 family members. In zebrafish, the "early epiboly arrest" phenotype of *nrz* morphants could be rescued by coinjecting, together with the *nrz* antisense morpholino, in vitro synthesized mRNAs encoding full-length Nrz (mortality at 10 hpf: 7.2% ± 4.8%; n = 158) but not the ΔTM truncated protein devoid of its C-terminal membrane insertion domain (mortality at 10 hpf: 49.8% ± 18.8%; n = 106) (Figures 2C and 2D). This suggested that the interaction of Nrz with biological membranes was required for epiboly. To study the role of the membrane-associated pools of Nrz in more detail, two recombinant Nrz proteins were designed by replacing the native C-terminal TM domain by either the CytB5 ER-addressing TM domain (NrzCytB5) or the MaoB mitochondrial-addressing domain (NrzMaoB). The subcellular localization of both recombinant proteins as well as their ability to prevent zBax-induced cell death was checked in cultured cells before expressing in zebrafish embryo (Figures S2B–S2F). Surprisingly, complementation experiments with the corresponding in vitro synthesized mRNAs showed that the mortality of *nrz* morphants was not significantly prevented by NrzMaoB (mortality at 10 hpf: 41.2% ± 10.8%; n = 132), whereas NrzCytB5 prevented embryonic mortality with the same efficacy as the native Nrz protein (mortality at 10 hpf: 8.2% ± 4.7%; n = 170) (Figure 2D). Of note, ectopically expressed NrzCytB5 was able to prevent the constriction of the margin in *nrz* morphants (data not shown) suggesting that ER localization of Nrz is important for its function.

To further understand Nrz implication during development, we analyzed the consequences of *nrz* knockdown on the status of YSL mitochondria using Mitotracker. Indeed, in *nrz* morphants, the labeling of the YSL mitochondria with Mitotracker, was significantly decreased (Figures 2E, 2F, and 2I). Moreover, as shown by western blotting using protein extracts from purified YSL mitochondria, the loss of Nrz protein was correlated with cytochrome *c* release (Figure 2J). Thus, the downregulation of *nrz* expression resulted in both the dissipation of $\Delta\Psi_m$ and the release of cytochrome *c* from the YSL mitochondria. In *nrz* morphants, ectopic expression of either NrzCytB5 or NrzMaoB was able to prevent cytochrome *c* release from YSL mitochondria (Figure 2J), while NrzCytB5 was found to prevent $\Delta\Psi_m$ drop more efficiently, compared to NrzMaoB (Figures 2E–2I). Together, these results confirmed that the ER localization of Nrz is critical during early development; in addition, they suggested that the observed mitochondrial alterations could be triggered by a signal originating from the ER.

(G) Subcellular fractionation of YSL mitochondria and YSL ER of ER-GFP-expressing embryos (75% epiboly). Nrz is detected in the endoplasmic reticulum fraction (ER) and to a lesser extent in the mitochondrial fraction (Mito), being absent in the cytosolic fraction (SN). VDAC and GFP antibodies were used as mitochondrial marker and ER marker, respectively. See also Figure S1.

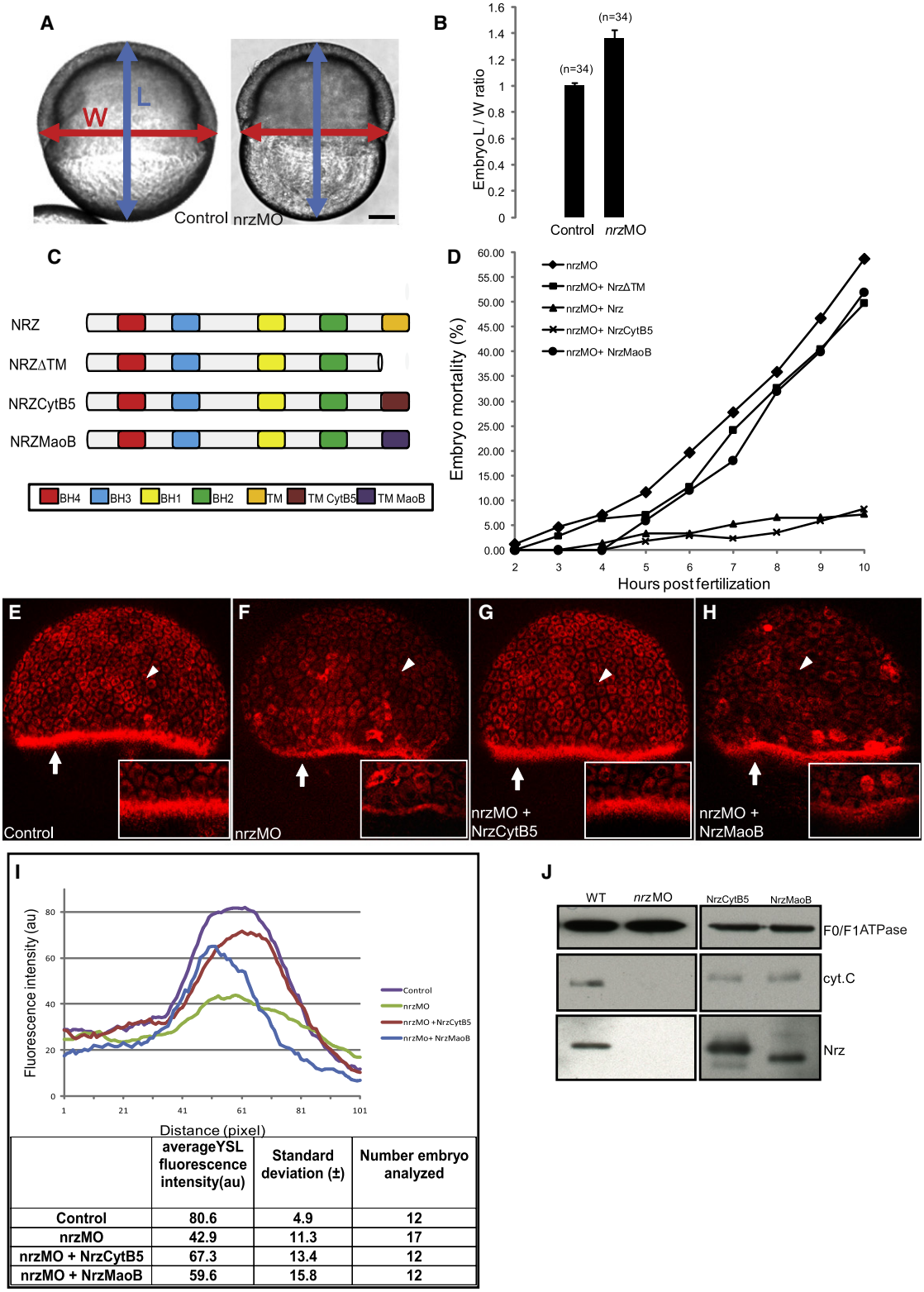

	averageYSL fluorescence intensity(au)	Standard deviation (±)	Number embryo analyzed
Control	80.6	4.9	12
nrzMO	42.9	11.3	17
nrzMO + NrzCytB5	67.3	13.4	12
nrzMO + NrzMaoB	59.6	15.8	12

Figure 2. Effect of *nrz* Knockdown and Nrz Subcellular Localization on Epiboly and YSL Mitochondria

(A) Embryo length (L) and width (W) used for calculating the L/W ratio; left: control embryo; right: *nrz* morphant.

(B) Histogram showing the L/W ratio of control embryos (WT) and *nrz* morphants (*nrz*MO) at 50% epiboly/shield stage (mean ± SD; three independent experiments; $p < 0.01$).

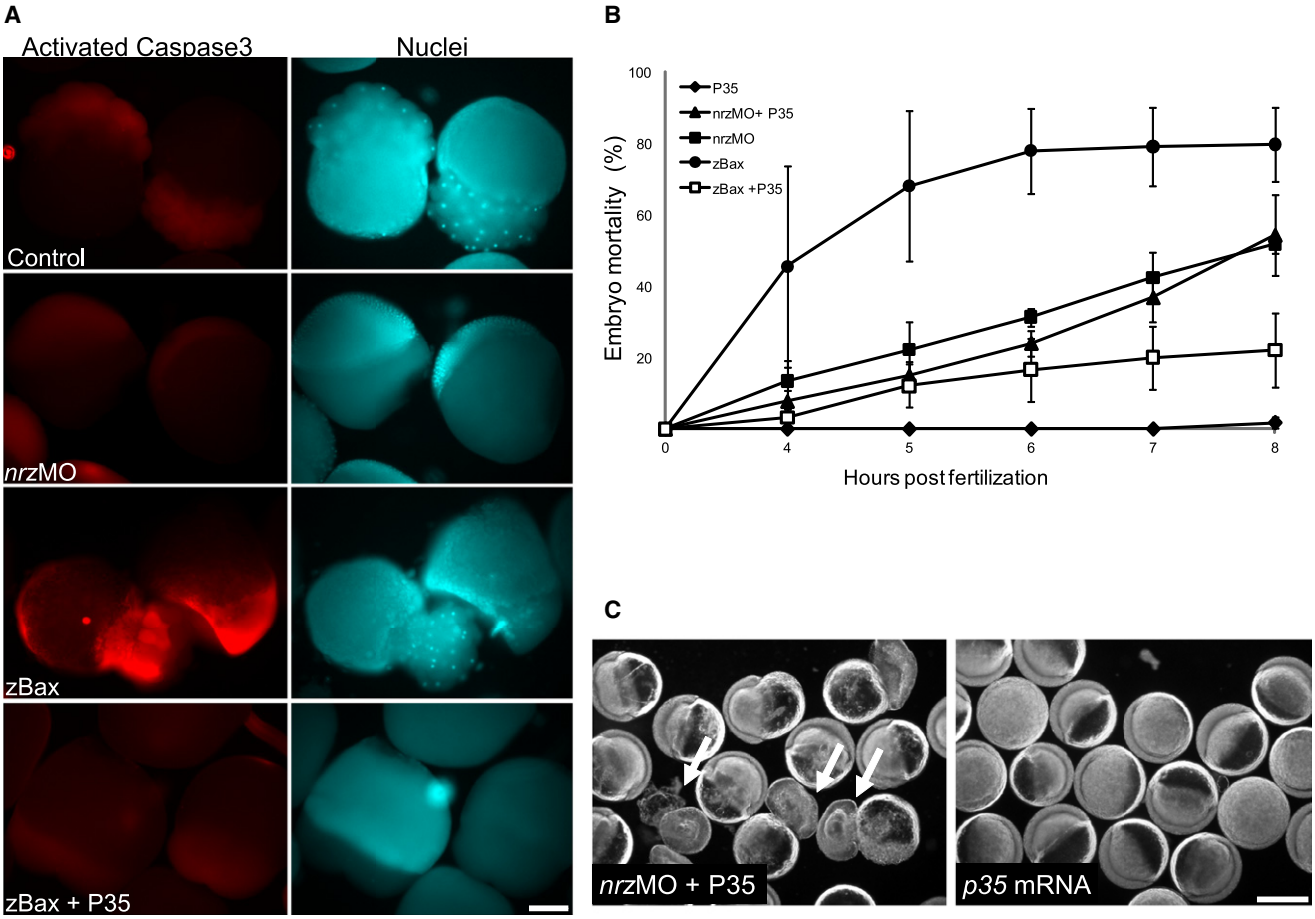

Figure 3. *Nrz* Knockdown Results in Caspase-Independent Epiboly Arrest

(A) Left panels: activated caspase-3 staining of embryos injected at the one cell stage with *egfp* mRNA (control), *nrz*MO (0.5 mM), *zbax* mRNA, or *zbax* mRNA plus *p35* mRNA. *Zbax*-expressing embryos were stained at the two to eight cell stage, whereas *nrz* morphants were labeled at the 30%–50% epiboly stage. Right panels: same embryos stained with Hoechst's reagent to visualize nuclei. Scale bar: 200 μm.

(B) Mortality rate of control zebrafish embryos injected with *p35* and *zbax* mRNA either alone or in combination and of *nrz* morphants coinjected or not with p35 mRNA (mean ± SD; three independent experiments).

(C) Bright-field images showing the phenotype of control embryos and *nrz* morphants injected with p35 mRNA. Scale bar: 500 μm.

Nrz Knockdown Results in Epiboly Arrest Independently of Caspase Activation

Together, the above observations suggested that in the YSL mitochondria, the loss of Nrz protein elicited typical features of apoptosis, such as cytochrome *c* release and $\Delta\Psi_m$ dissipation. This prompted us to check whether or not the early lethal phenotype of *nrz* morphants was the consequence of caspase activation in the YSL. To address this issue, we used a specific antibody to detect the activated form of caspase-3 in embryos at the 30%–50% epiboly stage. As depicted in Figure 3A, knockdown of *nrz* did not appear to result in caspase-3 activation at this developmental stage (0% embryos with activated

(C) Schematic drawing of recombinant proteins. Nrz, full-length protein; NrzΔTM, deletion mutant lacking the TM domain; NrzCytB5, swap mutant with ER-addressing domain; NrzMaoB, swap mutant with mitochondria-addressing domain. BH and TM domains are shown as color boxes.

(D) Complementation experiments: Embryos were injected with *nrz* morpholinos to dampen endogenous *nrz* level and coinjected with mRNAs expressing the recombinant proteins displayed in (C). Embryo mortality (%) was measured at indicated (hours postfertilization). Representative data from 2–8 independent experiments. The *nrz* morpholino is directed against the 5′ untranslated region of the endogenous *nrz* mRNA; it does not match with the foreign *nrz* transcripts.

(E–H) Representative confocal images of Mitotracker Red-stained embryos injected with control morpholino (E), *nrz*MO morpholino (F), *nrz*MO + *nrzcytb5* mRNA (G), or *nrz*MO + *nrzmaob* mRNA (H); *nrz*MO-injected embryos exhibit a dramatic decrease in the labeling of the YSL mitochondria belt (white arrows).

(I) Quantitative analysis of Mitotracker labeling of zebrafish embryos. Fluorescence intensity is represented as a function of the distance from the animal pole (upper panel). Intensity peaks in the region of the YSL. Statistical data are shown (bottom panel).

(J) Immunoblot analysis of Nrz protein and cytochrome *c* contents of purified YSL mitochondria; F0/F1 ATPase was used as a loading control. Left: mitochondrial protein extracts from control embryos and *nrz* morphants; loss of Nrz protein correlates with cytochrome *c* release. Right: same analysis carried out on *nrz* morphants coinjected with mRNAs expressing NrzCytB5 or NrzMaoB; cytochrome *c* release appears to be prevented by both Nrz swap mutants. See also Movie S1 and Figure S2.

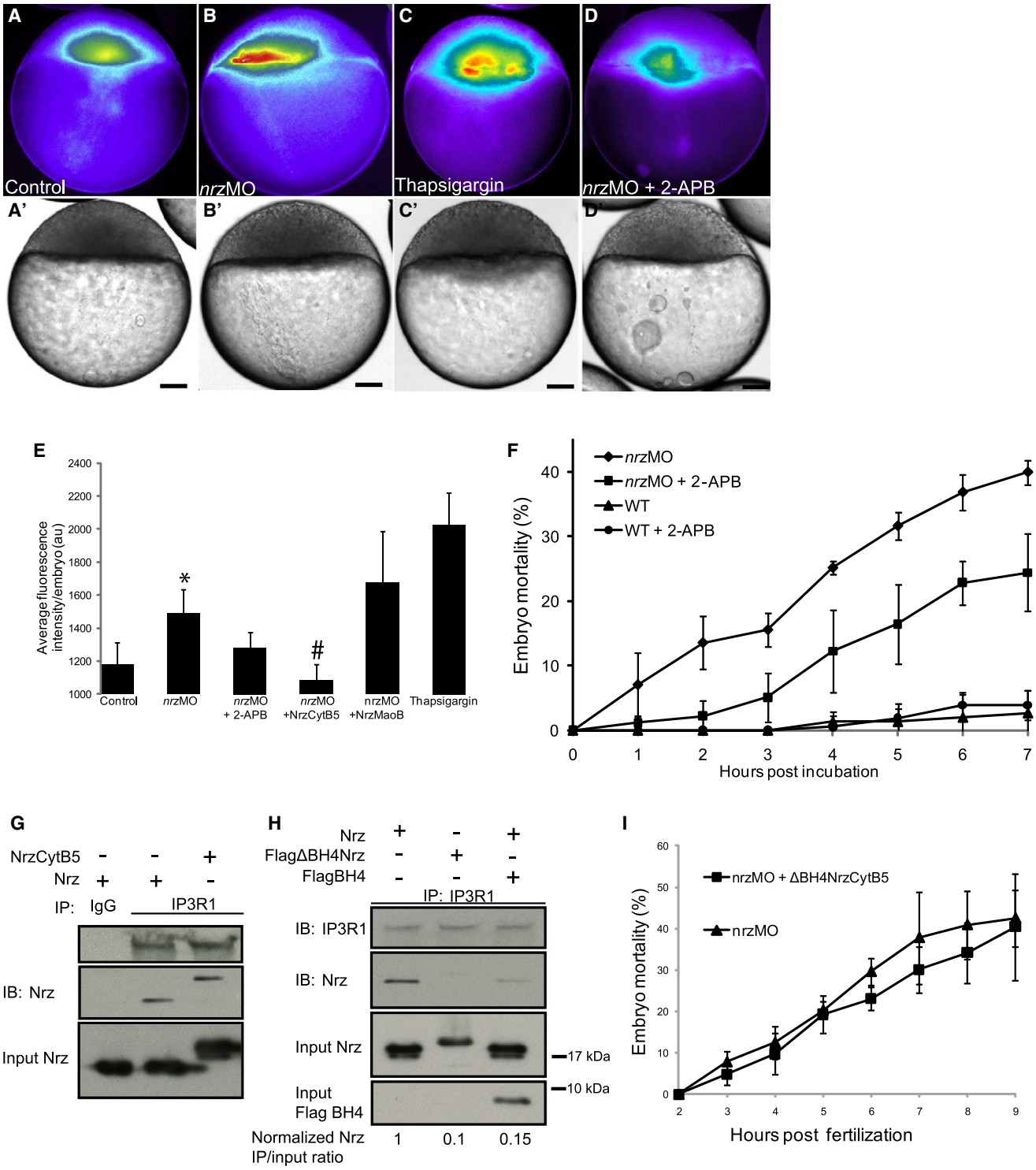

Figure 4. *Nrz* Binds to IP3R1 via Its BH4 Domain and Controls Intracellular Ca^{2+} Levels in Zebrafish Embryos

(A–D) Fluorescence microscopy images of control embryos (A), *nrz* morphants (B), WT embryos treated with thapsigargin (C), or *nrz* morphants treated with or 2-APB (D); embryos were stained with Oregon Green BAPTA-1 AM (false colors, oblong-sphere stage). Increased signal in thapsigargin-treated embryos and *nrz* morphants reveals the release of free Ca^{2+} in the region of the margin from which originates the YSL. In (A′–D′), bright-field images of the same embryos are shown. Scale bar: 100 μm.

(E) Quantification of Oregon Green BAPTA-1 AM staining of control embryos and of *nrz* morphants injected or not with *nrzcytb5* or *nrzmaob* mRNAs or treated with 2-APB (50 μM); embryos treated with thapsigargin alone (20 μM) were used as positive controls (mean ± SD; three independent experiments; *$p < 0.01$ versus control embryos; #$p > 0.9$ versus control embryos).

caspase-3, n = 10); in contrast, overexpression of the cell death accelerator zBax efficiently induced caspase activation as early as the four to eight cell stage (80% embryos with activated caspase-3; n = 10). In addition, apoptotic features downstream of caspase-3 activation such as chromatin condensation and formation of pyknotic nuclei were not observed in *nrz* morphants (data not shown). Finally, whereas the caspase inhibitor p35, prevented caspase-3 activation and subsequent embryonic lethality caused by ectopic expression of zBax, p35 was incapable to restore epiboly progression in *nrz* morphants (Figures 3B and 3C).

Together, these observations showed that, although the caspase-dependent cell death machinery already seems to be functional at early developmental stages in the zebrafish embryo, it was not activated following *nrz* knockdown. Thus, the premature arrest of epiboly observed in *nrz* morphants did not appear to be the consequence of caspase activation.

Nrz Knockdown Triggers IP3R-Dependent Intracellular Ca^{2+}Increase

The fact that the phenotype of *nrz* morphants was reverted by expressing NrzCytB5 protein was an indication of the contribution of the ER and raised the idea that Ca^{2+} flows inside the YSL might be altered following *nrz* knockdown. We thus evaluated the effect of *nrz* knockdown on the YSL Ca^{2+} levels using a dedicated fluorescent dye (Oregon Green, BAPTA-1). As shown in Figures 4A and 4B, knockdown of *nrz* resulted in a significant increase in "cytosolic" Ca^{2+} in the region of the margin (average fluorescence intensity [afi]: 1487.5 ± 146, n = 10), as compared with control embryos (afi: 1177.8 ± 135.7; n = 9). This increase was observed as early as the oblong-sphere stage, shortly before the start of the epiboly process. In addition, the observed Ca^{2+} peak was fully suppressed by expression of NrzCytB5 (afi: 1083.3 ± 96.1, n = 10), which was previously found to prevent the premature death of *nrz* morphants, contrary to NrzMaoB (afi: 1674.1 ± 311; n = 10), which was unable to restore the viability of *nrz* morphants (Figure 4E, see also Figure 2D). To further establish that the increase of YSL Ca^{2+} concentration is a causal event of the observed epiboly arrest in *nrz* morphants, zebrafish embryos were treated with the SERCA inhibitor thapsigargin (512 cell stage), which is routinely used to induce cytosolic Ca^{2+} accumulation in cultured cells. As shown in Figure 4C, thapsigargin treatment led to massive increase in Ca^{2+} concentration in the YSL, as similarly observed in *nrz* morphants. Moreover, embryos incubated with thapsigargin (5–20 μM) exhibited delayed epiboly; however, a limited number of embryos died prematurely, compared with *nrz* morphants (less than 5%, data not shown). Direct injection of thapsigargin into the YSL at the sphere-oblong stage considerably increased the rate of early mortality. Interestingly, thapsigargin treatment also led to $\Delta\Psi_m$ drop and cytochrome *c* release, thus phenocopying *nrz* morphants (Figures S5A–S5C).

As the observed Ca^{2+} increase in *nrz* morphants seems to originate from the ER we investigated the implication of the major calcium channel IP3R in the *nrz* knockdown phenotype. For this purpose, *nrz* morphants were incubated with the IP3R inhibitor 2-aminoethoxydiphenyl borate (2-APB). Prolonged treatment of embryos with 2-APB throughout epiboly significantly delayed epiboly progression (Figure S3D); thus, *nrz* morphants were transiently incubated with 2-APB (from 512 cells to oblong stage). In such conditions, as shown in Figures 4D and 4E, 2-APB treatment prevented the increase of Ca^{2+} levels in *nrz* morphants (afi: 1195.6 ± 155; n = 19). Moreover, as shown in Figure 4F, early mortality was significantly reduced in *nrz* morphants upon 2-APB treatment (*nrz*MO embryos: mortality at 10 hpf = 39.9% ± 1.9%; 2-APB treated *nrz*MO embryos: mortality at 10 hpf = 24.4% ± 6%). Interestingly, heparin as well as Xestospongin C, two other inhibitors of IP3R, have a similar effect (Figures S3E and S3F). This suggested that the Ca^{2+} increase observed in *nrz* morphants is IP3R dependent.

Nrz Interacts with the IP3R1 Channel via Its BH4 Domain

It was previously shown that the Bcl-2 protein can regulate cytosolic Ca^{2+} concentrations via its interaction with the IP3R1 Inositol 1,4,5-triphosphate receptor channel; moreover, Bcl-2 was reported to interact directly with IP3R1 via its BH4 domain (Rong et al., 2009). To directly check if Nrz was able to repress the opening of the IP3R1 channel, the effect of Nrz on the release of calcium originating from the ER was studied in HeLa cells following histamine treatment, which is known to trigger calcium release into the cytosol by increasing intracellular IP3 levels. Indeed, full-length Nrz, as well as NrzCytB5, but not ΔBH4NrzCytB5, prevented histamine-dependent Ca^{2+} release (Figures S3G and S3H). To check if Nrz interacted with IP3R1 via its BH4 domain, a series of Nrz mutants were expressed in HeLa cells, Nrz/IP3R1 interactions being detected by co-immunoprecipitation and western blotting. As shown in Figure 4G, whole-length Nrz did interact with IP3R1 as well as ER-addressed NrzCytB5; in contrast, no interaction could be detected with ΔBH4Nrz, whereas the BH4 domain alone appeared to disrupt Nrz/IP3R1 interaction (Figure 4H). Finally, the fact that in *nrz* morphants, contrary to full-length NrzCytB5 (Figure 2B), ΔBH4NrzCytB5 neither restored epiboly progression (Figure 4I) nor prevented the increase of Ca^{2+} in the YSL (data not shown) was an indication that the observed interaction between IP3R1 and Nrz was of functional significance.

Nrz Knockdown Alters the Cytoskeleton in the Yolk Cell

The yolk cell and in particular the YSL is a dynamic structure containing a broad range of cytoskeleton components that organize

(F) Effect of IP3R inhibition with 2-APB on the mortality of zebrafish embryos. Control embryos (WT) and *nrz* morphants (MO) were incubated or not with 2-APB (50 μM) from 512 cells to oblong-sphere stage. Mortality was evaluated at indicated times after the beginning of the incubation (mean ± SD; three independent experiments).

(G and H) Immunoprecipitation experiments with protein extracts from transfected HeLa cells: Nrz and NrzCytB5 coimmunoprecipitated with the IP3R1 channel (G); Nrz but not ΔBH4Nrz was able to interact with IP3R1 (H); the Flag-tagged BH4 peptide domain inhibited Nrz/IP3R1 interaction. Bottom: densitometry quantification, Nrz IP/input ratios obtained by calculating the ratio of IP band intensity (lanes "IB:Nrz") to the input band intensity (lanes "Input Nrz").

(I) Time course analysis of *nrz* morphants injected or not with in vitro synthesized ΔBH4NrzCytB5 mRNA. Ectopic expression of ΔBH4NrzCytB5 is unable to prevent *nrz*MO lethal phenotype (mean ± SD; three independent experiments). See also Figure S3.

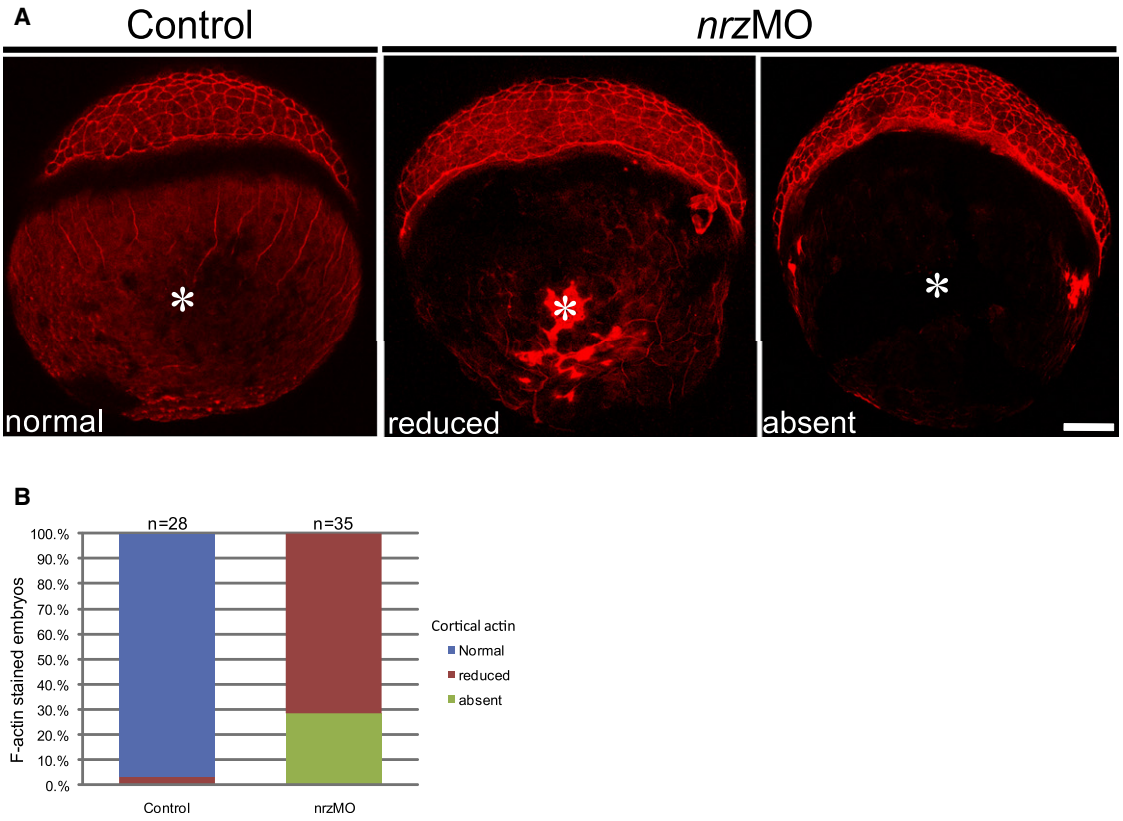

Figure 5. *Nrz* Knockdown Leads to Profound Alterations of the Cytoskeleton Inside the Yolk Cell

(A) F-actin staining in control embryos and *nrz* morphants at 40%–50% epiboly stage showing the status of cortical F-actin inside the vegetal pole (white asterisk). In *nrz* morphants, cortical actin is severely reduced or absent.

(B) Histogram showing the percentage of control embryos versus *nrz* morphants at 50% epiboly stage with normal (blue), reduced (red), or absent (green) cortical F-actin. See also Figure S4.

into complex networks of microtubules and microfilaments (cortical F-actin, actin-myosin ring). These networks actively drive epiboly progression during early development (Cheng et al., 2004; Koppen et al., 2006). Ca^{2+} is a major intracellular messenger that controls a variety of cellular processes including cytoskeleton remodeling and morphogenesis; it plays a critical role throughout the development of the zebrafish (Ashworth et al., 2007; Gilland et al., 1999; Webb and Miller, 2006; Westfall et al., 2003). Ca^{2+} fluxes in the vicinity of the margin were recently suggested to participate in epiboly (for review, see Webb and Miller, 2006). Thus, the effect of *nrz* knockdown on the cytoskeleton of the yolk cell was analyzed. Microtubules appeared to be intact in the blastomeres of *nrz* morphants. In contrast, the microtubule network was dramatically disorganized in the yolk cell; this effect being prevented by the microtubule stabilizing agent Taxol (Figures S4A–S4C). However Taxol did not prevent the mortality of *nrz* morphants (data not shown). This suggested that Nrz was required for the YSL microtubule stability during epiboly but that the observed disorganization of the microtubule network in the yolk cell of *nrz* morphants was the consequence rather than the cause of early embryonic mortality.

We then analyzed the effect of *nrz* knockdown on the organization of the F-actin network using phalloidin-rhodamine staining. In control embryos, a diffuse signal was detected in the yolk cell, corresponding to cortical actin (Cheng et al., 2004). Remarkably, this signal was severely altered, being reduced (71.4%, n = 35) or even suppressed (28.6%) in *nrz* morphants as compared to control embryos (96.4% normal, n = 28) (Figure 5). The observed cortical actin disruption appeared to be possibly due to both F-actin depolymerization and partial proteolytic degradation (Figure S4D).

Thus, knockdown of *nrz* resulted in alterations both in actin microfilaments and microtubules in the yolk cell. By contrast, in the animal pole, apart from the blastomeres in direct contact with the margin, the overall organization of the cytoskeleton did not seem to have been altered (Figures 5 and S4D).

Effect of *nrz* Knockdown Triggers MLCK-Dependent Actin-Myosin Complex Formation at the Margin

During zebrafish development an actin-myosin ring forms at 75% epiboly and plays an essential role in epiboly progression and blastopore closure (Cheng et al., 2004; Rohde and Heisenberg, 2007). This raised the possibility that in *nrz* morphants, the observed constriction of the margin could be due to premature formation of the actin-myosin complex. Indeed, as shown in Figure 6A, the actin-myosin ring had already appeared

when the margin reached the yolk cell equator (50% epiboly), whereas in control embryos this structure was not present until 75% epiboly. It should be noted that the treatment of *nrz* morphants with the selective myosin II inhibitor blebbistatin, significantly delayed the constriction of the margin in *nrz* morphants (data not shown). These observations suggested that in *nrz* morphants, the constriction of the actin-myosin ring was accelerated, whereas the speed of progression of the margin down to the vegetal pole was unchanged. Importantly, thapsigargin-treated embryos exhibited similar early margin constriction as well as premature formation of the actin-myosin ring (Figure 6A), suggesting that in *nrz* morphants as well, these events are the consequence of massive Ca^{2+} release from the ER inside the yolk cell. Finally, overexpression of Nrz appeared to prevent the formation of the actin-myosin ring and delay epiboly (Figure S5).

At the molecular level, the formation of the actin-myosin complex is triggered by the phosphorylation of MLC subunits (Thr-18 and Ser-19 residues) (Matsumura, 2005). We thus analyzed MLC phosphorylation in *nrz* morphants by immunofluorescence and western blotting, using an antibody specific for phosphorylated Ser-19. Remarkably, at 50% epiboly, such phosphorylation was observed at the leading edge of the margin in *nrz* morphants (actin-myosin ring positive embryos = 76.9%, n = 13), but not in control embryos (0%, n = 14) (Figure 6B). In addition, protein extracts from *nrz* morphants showed increased myosin phosphorylation (Figure 6C), raising the possibility that the formation of the actin-myosin ring in *nrz* morphants may be the consequence of premature phosphorylation of MLC. Interestingly, thapsigargin treatment of zebrafish embryos induced a similar increase of Ser-19 phosphorylation in a dose dependant manner (Figure 6C), suggesting that MLC phosphorylation depends on the release of Ca^{2+} from the ER inside the YSL.

Two main kinases are capable of phosphorylating MLC directly at Ser-19: MLCK and Rho-associated protein kinase 1/2 (ROCK 1/2) (Matsumura, 2005; Takashima, 2009; Totsukawa et al., 2000). In zebrafish, these kinases are both expressed during early development (Blaser et al., 2006). We thus evaluated their involvement in the phenotype of *nrz* morphants, using specific inhibitors. As shown in Figure 6D, incubation with the MLCK inhibitor ML-7 slowed down the mortality of *nrz* morphants significantly (mortality at 7 hpf = 4.4% ± 6.2%, n = 59), whereas the ROCK inhibitor Y26732 had little or no effect (mortality at 7 hpf = 23.8% ± 8.3%, n = 62). In addition, the MLCK inhibitor ML-7 (actin ring positive embryos [RPE] = 20%, n = 15), as well as the calmodulin antagonist W13 (RPE = 14.3%, n = 14), prevented MLC phosphorylation and premature actin ring formation in *nrz* morphants (Figure 6B), contrary to Y26732, which had no effect (RPE = 75%, n = 12). Together, these results suggested that calmodulin-dependent MLCK activity was required for premature formation of the actin-myosin ring observed in *nrz* morphants.

Altogether, these data indicated that *nrz* invalidation results in the massive release of Ca^{2+} from ER stores, which then triggers MLC phosphorylation via MLCK. As a result, the formation of the contractile actin-myosin ring occurs prematurely, leading to the detachment of the blastomeres from the yolk cell and death of the embryo (Figure 7).

DISCUSSION

In the zebrafish, epiboly is driven by the cytoskeletal dynamics of the YSL and of the migrating blastomeres as well as presumably by active endocytosis events at the level of the blastomere plasma membrane. The formation of a contractile actin-myosin ring, in the region of the margin, is critical for epiboly completion (Solnica-Krezel, 2006). These events seem to be orchestrated in part by Ca^{2+} transients, the underlying molecular mechanisms remaining largely unknown (Webb and Miller, 2006).

Effect of *nrz* Knockdown on YSL Mitochondria

We previously showed that the knockdown of the apoptosis inhibitor *nrz* led to premature epiboly arrest. In the zebrafish embryo, the *nrz* transcript is specifically accumulated in the YSL. Here, we demonstrate that the YSL contains a dense ER network and a large number of active mitochondria. Our results show that Nrz protein is localized to both YSL ER and mitochondria.

Of note, *nrz* knockdown affects the TM potential of YSL mitochondria, and to a lesser extent of the blastomere mitochondria. The observed $\Delta\Psi_m$ dropdown is accompanied by the release of cytochrome *c* but not by any detectable activation of caspase-3. However, expression of the caspase inhibitor p35 could not prevent the early mortality caused by *nrz* downregulation. Thus, the phenotype caused by the knockdown of *nrz* appears to be caspase independent.

Effect of *nrz* Knockdown on Ca^{2+} Fluxes in the YSL

The localization of Nrz in the ER, but not in mitochondria, is critical for the proper early development of the embryo. Indeed, *nrz* knockdown leads to a marked increase in cytosolic Ca^{2+} levels in the YSL, which is prevented by ectopically expressed ER-addressed NrzCytB5, but not by mitochondria-addressed NrzMaoB. Moreover, artificial increase of free Ca^{2+} in the YSL upon thapsigargin treatment of zebrafish embryos phenocopies *nrz* morphants. Of note, thapsigargin treatment also results in a decrease in transmembrane potential of YSL mitochondria and triggers cytochrome *c* release. The interplay between Ca^{2+} signaling and mitochondrial status has been extensively studied; mitochondria are capable of storing substantial amounts of Ca^{2+}, thus playing the role of intracellular Ca^{2+} buffer (Rizzuto et al., 2009). Treating the cells, including thapsigargin, with cytotoxic agents, triggering a massive release of Ca^{2+} into the cytosol generally ends in cell death (Rong and Distelhorst, 2008). Calcium waves observed in *nrz* morphants seem to originate from the margin, thus affecting primarily YSL mitochondria. However, blastomere mitochondria may be also affected due to Ca^{2+} entry from the YSL via the gap junctions located into their plasma membrane (Webb and Miller, 2006).

The effects of Bcl-2 family members on intracellular Ca^{2+} fluxes are still under active investigation. It has been reported that Bcl-2 and Bcl-xL could increase calcium leak from the ER thus reducing the amount of calcium available for inducing apoptosis (White et al., 2005; Rizzuto et al., 2009). Alternatively, Bcl-2 was shown to interact with the IP3R1 Ca^{2+} channel and prevent the release of Ca^{2+} from the ER thus preventing Ca^{2+} overloading of the mitochondria and downstream apoptosis events (Rong et al., 2009).

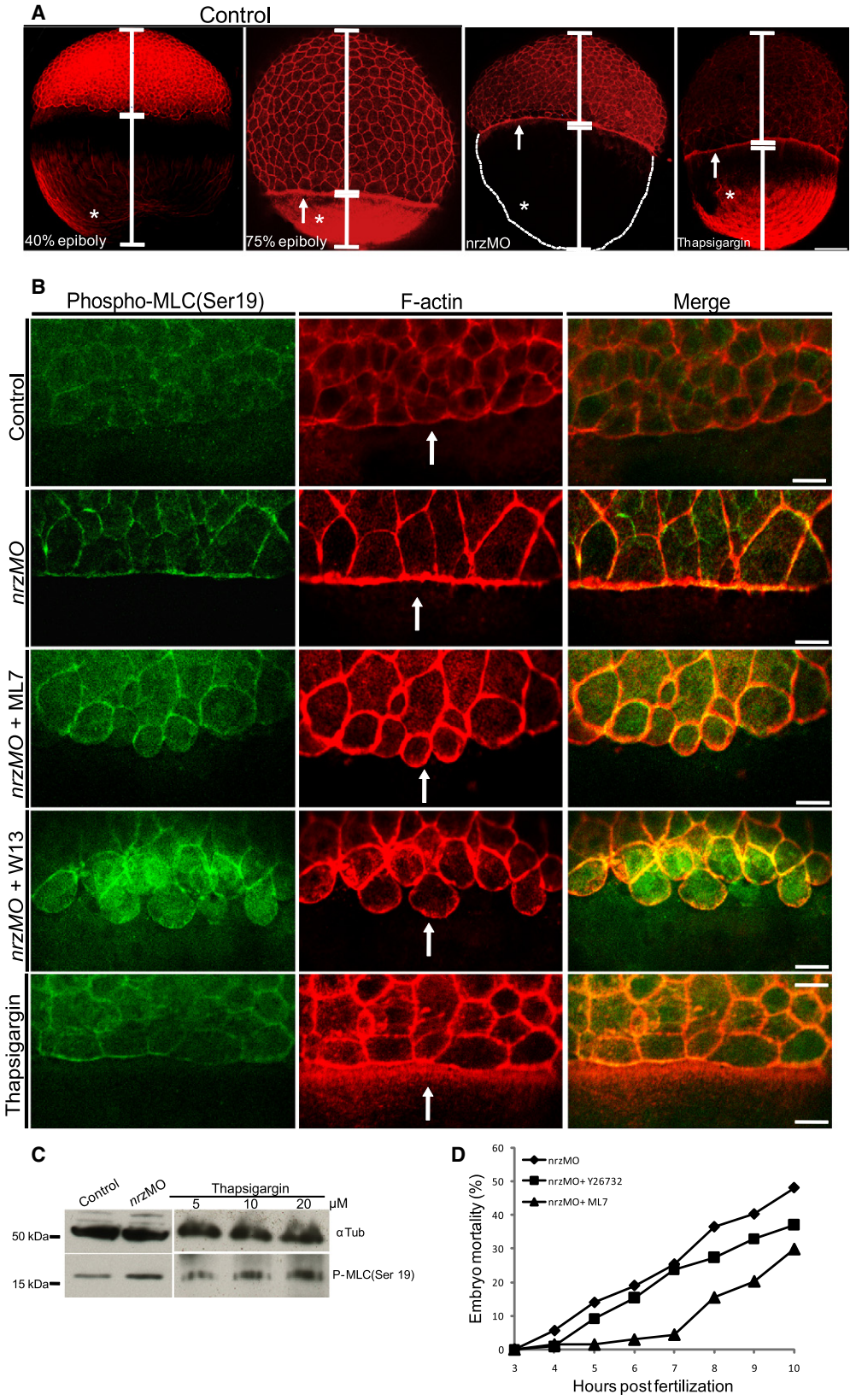
A
Control
40% epiboly
75% epiboly
nrzMO
Thapsigargin
B
Phospho-MLC(Ser19)
F-actin
Merge
Control
nrzMO
nrzMO + ML7
nrzMO + W13
Thapsigargin
C
Control
nrzMO
Thapsigargin
5
10
20
μM
50 kDa
15 kDa
α Tub
P-MLC(Ser 19)
D
nrzMO
nrzMO+ Y26732
nrzMO+ ML7
Embryo mortality (%)
Hours post fertilization

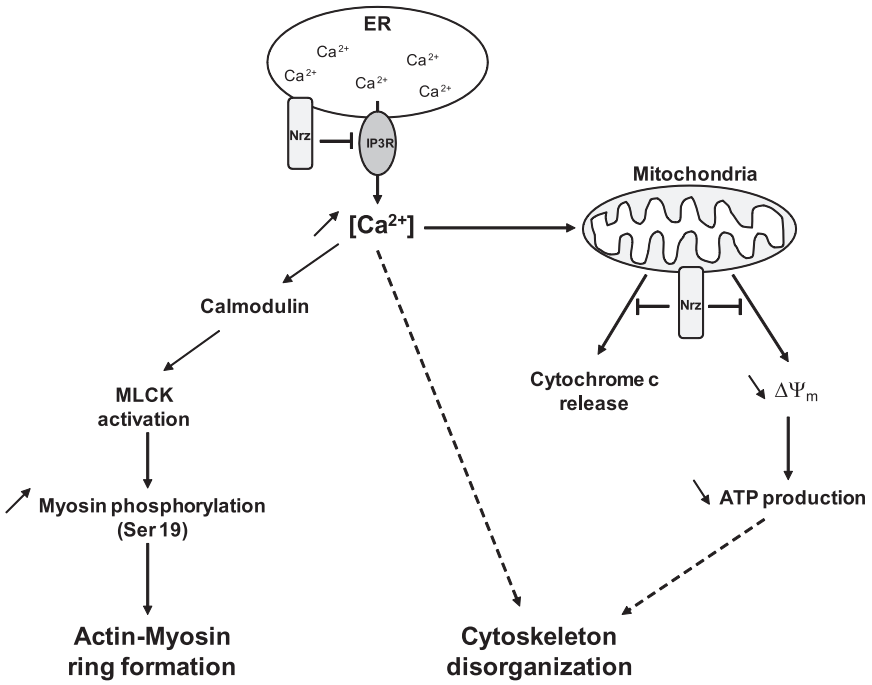

Figure 7. A Model for the Role of Nrz in the YSL during Zebrafish Development

Nrz located to the ER is critical for the regulation of YSL Ca^{2+} fluxes. *Nrz* knockdown increases YSL free Ca^{2+} levels, leading to MLC hyperphosphorylation presumably via calmodulin/MLCK pathway, premature actin-myosin ring formation, and subsequent YSL cytoskeletal breakdown. Ca^{2+} may also directly lead to microtubule depolymerization, as their stability is compromised in the presence of increased Ca^{2+} levels. Another consequence of free Ca^{2+} increase is the alteration of the YSL mitochondria as shown by $\Delta\Psi_m$ loss and cytochrome *c* release. The alteration of the mitochondrial status may also contribute to cytoskeletal disorganization due to decreased production of ATP into the YSL.

Our data suggest that Nrz regulates YSL Ca^{2+} levels by interacting with the IP3R1 channels via its BH4 domain. This interaction appears to occur between the BH4 domain of Nrz and IP3R1. Whether this effect on YSL Ca^{2+} levels occurs exclusively in an IP3R-dependent manner or by an additional mechanism will require further studies.

Effect of *nrz* Knockdown on Cytoskeletal Dynamics in the YSL

The YSL contains a large number of cytoskeletal proteins that drive in part epiboly morphogenic movements (Cheng et al., 2004; Koppen et al., 2006). In *nrz* morphants, the microtubule network and F-actin vegetal actin are dramatically affected, which might result from a decrease in ATP concentrations in the yolk cell due to alterations of YSL mitochondria (Figures 2E–2J). However, these cytoskeletal modifications are more likely to be consequences rather than the actual cause of early mortality since they occur after the constriction of the margin. Our results suggest that the constriction of the margin and subsequent embryonic death are due to the premature formation of the contractile actin-myosin ring. Indeed, the contractile ring normally forms after the EVL reaches the equator (75% epiboly), which favors epiboly completion (Solnica-Krezel, 2006). In *nrz* morphants, the formation of the actin myosin ring occurs before the EVL reaches the equator, resulting in the detachment of the entire embryo from the yolk. Importantly, premature formation of the actin myosin ring is correlated with increased phosphorylation of MLC on Ser-19, which is known to enhance myosin ATPase activity and stress fibers formation (Totsukawa et al., 2000). The effect of the two pharmacological agents ML7 and Y26732 suggest that the inhibition of MLCK, but not ROCK1/2, significantly delays margin constriction and early mortality of Nrz morphants. In the smooth muscle, MLCK activation and myosin phosphorylation are Ca^{2+} dependent. The release of Ca^{2+} from the ER leads to the activation of the Ca^{2+}-dependent calmodulin protein, which subsequently binds and activates MLCK (Matsumura, 2005). We show here that W-13 treatment of *nrz* morphants inhibits premature actin-myosin ring formation, suggesting that similar calmodulin-dependent MLCK activation occurs at the margin.

In *nrz* morphants, the rise in Ca^{2+} levels leads to mitochondrial dysfunction and increased MLC phosphorylation by MLCK. Thus, it turns out that in addition to Nrz, the formation of the contractile ring is under the control of a multiplicity of factors,

Figure 6. *Nrz* Knockdown Leads to Increased Myosin Phosphorylation at the Margin and Premature Actin-Myosin Contractile Ring Formation

(A) F-actin staining of control embryos (40% and 75% epiboly), *nrz* morphants (*nrz*MO), and thapsigargin-treated (5 μM) embryos. In control embryos, the actin-myosin ring is present at 75% epiboly but absent at 40% epiboly (white arrows). In *nrz* morphants the actin-myosin ring is already present before migrating blastomeres reached the equator. White asterisks materialize the location of vegetal F-actin inside the yolk cell. Scale bar: 100 μm.

(B) Immunofluorescence analysis of the margin region of 50% epiboly stage embryos: staining of phospho-MLC of *nrz* morphants versus control embryos showing MLC phosphorylation at the margin in *nrz* morphants, which is correlated with an increase in the F-actin signal (phalloidin staining). Merged images are shown on the right. Treatment of *nrz* morphants with the MLCK inhibitor ML7 or the calmodulin antagonist W13 inhibits MLC phosphorylation and F-actin polymerization. Thapsigargin-treated embryos were used as positive controls. Scale bar, 20 μm. Representative data from at least three embryos (50% epiboly).

(C) Immunoblot analysis of the phospho-MLC (Ser-19) content in the blastoderm of control embryos, *nrz* morphants, and embryos treated with increasing amounts of thapsigargin.

(D) Effect of ROCK inhibitor Y26732 (50 μM) and MLCK inhibitor ML7 (20 μM) on the mortality of *nrz* morphants. Mortality of ML7-treated embryos 7 hpf results in blastomere detachment due to the lack of actin-myosin ring formation. Representative results from three independent experiments are shown. See also Figure S5.

including the MTX2 transcription factor (Wilkins et al., 2008), the MAPKAPK2 protein kinase (Holloway et al., 2009), the Ste20 like kinase MSN1 (Koppen et al., 2006), and the mDIA2 formin (Lai et al., 2008). Understanding of the interplay between the signaling pathways involved remains a major issue.

The Bcl-2 Family of Proteins as Regulators of Cytoskeleton Dynamics

Why the release of cytochrome *c* from the YSL mitochondria does not result in caspase activation remains an open question. The possibility exists that phosphorylation of MLC occurs shortly after the release of Ca^{2+} such that the contraction of the actin-myosin ring and subsequent separation of the blastomeres from the yolk cell may occur before caspases can be activated. This then raises the possibility that the Bcl-2 family of apoptosis regulators, via their effect on Ca^{2+} signaling, may indeed have multiple roles into the cell when apoptosis is silenced.

Actually, there may be a dual role for Nrz during epiboly, first in the ER, where it may participate, as shown in this report, in fine-tuning of the Ca^{2+} fluxes and ensure the formation of the actin ring at the right time; second, in the YSL mitochondria, where, possibly by enhancing their Ca^{2+} uptake capacity (see Murphy et al., 1996), it may preserve mitochondrial integrity by avoiding $\Delta\Psi_m$ drop and preventing cytochrome *c* release. Indeed, this could explain the observed capacity of NrzMaoB to prevent mitochondrial dysfunction in *nrz* morphants. Nrz may also prevent unwanted apoptotic events that may otherwise be triggered when the blastomeres merge and give rise to the YSL. Indeed, there is evidence that syncytium formation favors apoptosis spreading (Greenwood and Gautier, 2005; Huppertz et al., 2001). Finally, Nrz might be critical for the contribution of YSL mitochondria to the regulation of Ca^{2+} transients throughout epiboly.

Thus, our results suggest that Bcl-2 family members, in addition to their role in controlling apoptosis, may play a pivotal role in remodeling the cytoskeleton during cell migration, epithelial mesenchymal transition, and possibly metastasis formation.

EXPERIMENTAL PROCEDURES

Embryo Manipulation

Morpholino (0.5 mM) and mRNA (100 ng/μl) injections were performed at one to four cell stages. Thapsigargin (5–20 μM) was incubated at 1000 cell stage for 3 hr or injected in the YSL at oblong-sphere stage. ML-7 (20 μM), Y27632 (50 μM), and W-13 (100 μM) were incubated at oblong-sphere stage. For embryo mortality quantification, 50 μM 2-APB was added before MBT for 45 min (between 512 cells and oblong stage), which did not cause any significant early epiboly delay. After incubation, embryos were washed with egg water and mortality was evaluated.

Immunofluorescence Analysis and In Vivo Staining

Image acquisition was carried out with the same gain, amplification, and exposure time between each experimental condition and the corresponding control. Image analysis was done using ImageJ software. All the procedures were carried out at room temperature unless otherwise stated. For Ca^{2+} dynamics experiments, one cell stage embryos were injected with 10 μM Oregon Green 488 BAPTA-1 AM and analyzed at high stage using Nikon TE300 fluorescence microscope. Double phosphomyosin/F-actin and Nrz staining were carried out as described (Koppen et al., 2006). In brief, embryos at the desired stage were fixed overnight in 4% paraformaldehyde at 4°C and washed in 0.1% Triton in PBS (PBT). They were then permeabilized for 1 hr in 0.5% Triton in PBS and subsequently incubated in block solution (10% normal goat serum, 1% DMSO, 0.1% Triton in PBS). Embryos were then incubated overnight at 4°C with 1/100 rabbit antiphospho-MLC 2 Ser-19 or 1/100 rabbit anti-Nrz antibody. Following three washes in PBT, embryos were incubated in Phalloidin and/or secondary antibodies and incubated overnight at 4°C. In vivo active mitochondria staining was performed by incubating embryos at the 40% epiboly stage with Mitotracker Red (500 nM) in egg water for 30 min at 28.5°C. Embryos were then washed extensively with egg water and visualized using a confocal microscope Axiovert 100M LSM510. The YSL ER was visualized in vivo by injecting 100 μM ER tracker at one cell stage or injecting *egfpcytb5* mRNA. Activated caspase-3 staining was performed as described (Jette et al., 2008).

Subcellular Fractionation

All steps were carried out at 4°C if not otherwise stated. Mitochondria and ER localized to the YSL were purified as follows: approximately 100–150 embryos were put in 1 ml cold MB buffer (210 mM mannitol, 70 mM sucrose, 1 mM EDTA, 10 mM HEPES [pH 7.5] containing proteases inhibitors) and the yolk sac disrupted with a P1000 tip. Embryos were then shaken for 5 min at 1100 rpm to dissolve the yolk and then centrifuged 2 min at 300 × *g* to pellet the blastomeres. The supernatant was centrifuged at 1500 × *g* twice for 5 min each to eliminate yolk nuclei and then centrifuged at 10,600 × *g* for 5 min. The pellet containing mitochondria was washed once with MB buffer and prepared for further analyses. The supernatant was then centrifuged at 100,000 × *g* for 1 hr. The supernatant containing cytosolic fraction was conserved and the pellet was resuspended in RIPA buffer for further analyses.

For HeLa cell fractionation, cells at 90% confluence in 10 cm^2 plates were transfected with pCS2+-NrzCytB5 or pCS2+-NrzMaoB using lipofectamine transfection reagent. Twenty-four hours after transfection, mitochondria were purified using the Qproteome Mitochondria Isolation Kit (QIAGEN) according to manufacturer recommendation. After mitochondria isolation, the ER was purified from the supernatant as described above.

Immunoprecipitations and Immunoblotting

For IP3R/Nrz coimmunoprecipitation experiments, 4 × 10^6 HeLa cells were transfected with the corresponding vector. Cells were then lysed in TNE buffer (10 mM Tris-HCl, 200 mM NaCl, 1 mM EDTA [pH 7.4], 1 mM β glycerophosphate, 1 mM orthovanadate, 0.1 mM sodium pyrophosphate containing protease inhibitors). Extracts were precleared with protein G-Sepharose beads for 1 hr and then incubated with 6 μg of primary anti-IP3R antibody. Extracts were then incubated with protein G-Sepharose beads for 2 hr. Immunoprecipitated fractions were washed five times with TNE and analyzed by immunoblotting. For yolk cortical actin, immunoprecipitation experiments were carried out on yolk fractions (see below) obtained from embryos at 40%–50% epiboly stage. Four micrograms of primary anti-α-actin antibody were used for the immunoprecipitation.

Ser-19 phosphorylation status of MLC was done on extracts from blastomeres separated from the yolk as described (Link et al., 2006). Proteins were extracted in RIPA buffer (1% NP-40, 0.5% deoxycholic acid, 0.1% SDS in PBS, containing protease and phosphatase inhibitors) and analyzed using anti-phospho-MLC (Ser-19) antibody (1/500 dilution). Detection of Nrz and cytochrome *c* was performed on protein extracts from isolated YSL mitochondria (50 embryos/ lane), using anti-Nrz (1/200) and anti-cytochrome *c* (1/500) antibodies.

Statistical Analysis

Error bars displayed on graphs represent mean ± SD of three independent experiments. Statistical significance was analyzed using Student's t test; $p < 0.01$ was considered significant.

SUPPLEMENTAL INFORMATION

Supplemental Information includes Supplemental Experimental Procedures, Supplemental References, five figures, and one movie and can be found with this article online at doi:10.1016/j.devcel.2011.03.016.

ACKNOWLEDGMENTS

We acknowledge A. Cornut for technical assistance as well as P. Gonzalo, J. Lopez, and A. Aouacheria for stimulating discussions. This work was

supported ARC and Ligue contre le Cancer. N.P. and B.B. are fellows from the Ministère de la Recherche.

Received: September 14, 2010
Revised: February 2, 2011
Accepted: March 21, 2011
Published: May 16, 2011

REFERENCES

Arnaud, E., Ferri, K.F., Thibaut, J., Haftek-Terreau, Z., Aouacheria, A., Le Guellec, D., Lorca, T., and Gillet, G. (2006). The zebrafish bcl-2 homologue Nrz controls development during somitogenesis and gastrulation via apoptosis-dependent and -independent mechanisms. Cell Death Differ. *13*, 1128–1137.

Ashworth, R., Devogelaere, B., Fabes, J., Tunwell, R.E., Koh, K.R., De Smedt, H., and Patel, S. (2007). Molecular and functional characterization of inositol trisphosphate receptors during early zebrafish development. J. Biol. Chem. *282*, 13984–13993.

Bivona, T.G., Quatela, S.E., Bodemann, B.O., Ahearn, I.M., Soskis, M.J., Mor, A., Miura, J., Wiener, H.H., Wright, L., and Saba, S.G.a. (2006). PKC regulates a farnesyl-electrostatic switch on K-Ras that promotes its association with Bcl-XL on mitochondria and induces apoptosis. Mol. Cell *21*, 481–493.

Blaser, H., Reichman-Fried, M., Castanon, I., Dumstrei, K., Marlow, F.L., Kawakami, K., Solnica-Krezel, L., Heisenberg, C.P., and Raz, E. (2006). Migration of zebrafish primordial germ cells: a role for myosin contraction and cytoplasmic flow. Dev. Cell *11*, 613–627.

Chen, R., Valentia, I., Zhong, F., McColl, K.S., Roderick, H., Bootman, M.D., Berridge, M.J., Conway, S.J., Holmes, A.B., Mignery, G.A., et al. (2004). Bcl-2 functionally interacts with inositol 1,4,5-trisphosphate receptors to regulate calcium release from the ER in response to inositol 1,4,5-trisphosphate. J. Cell Biol. *166*, 193–203.

Chen, Z.X., and Pervaiz, S. (2010). Involvement of cytochrome c oxidase subunits Va and Vb in the regulation of cancer cell metabolism by Bcl-2. Cell Death Differ. *17*, 408–420.

Cheng, J.C., Miller, A.L., and Webb, S.E. (2004). Organization and function of microfilaments during late epiboly in zebrafish embryos. Dev. Dyn. *231*, 313–323.

Chipuk, J.E., Moldoveanu, T., Llambi, F., Parsons, M.J., and Green, D.R. (2010). The BCL-2 family reunion. Mol. Cell *37*, 299–310.

de Moissac, D., Mustapha, S., Greenberg, A.H., and Kirshenbaum, L.A. (1998). Bcl-2 activates the transcription factor NFkappaB through the degradation of the cytoplasmic inhibitor IkappaBalpha. J. Biol. Chem. *273*, 23946–23951.

Gilland, E., Miller, A.L., Karplus, E., Baker, R., and Webb, S.E. (1999). Imaging of multicellular large-scale rhythmic calcium waves during zebrafish gastrulation. Proc. Natl. Acad. Sci. USA *96*, 157–161.

Greenwood, J., and Gautier, J. (2005). From oogenesis through gastrulation: developmental regulation of apoptosis. Semin. Cell Dev. Biol. *16*, 215–224.

Hengartner, M.O., and Horvitz, H.R. (1994). C. elegans cell survival gene ced-9 encodes a functional homolog of the mammalian proto-oncogene bcl-2. Cell *76*, 665–676.

Holloway, B.A., Gomez de la Torre Canny, S., Ye, Y., Slusarski, D.C., Freisinger, C.M., Dosch, R., Chou, M.M., Wagner, D.S., and Mullins, M.C. (2009). A novel role for MAPKAPK2 in morphogenesis during zebrafish development. PLoS Genet. *5*, e1000413.

Huppertz, B., Tews, D.S., and Kaufmann, P. (2001). Apoptosis and syncytial fusion in human placental trophoblast and skeletal muscle. Int. Rev. Cytol. *205*, 215–253.

Jette, C.A., Flanagan, A.M., Ryan, J., Pyati, U.J., Carbonneau, S., Stewart, R.A., Langenau, D.M., Look, A.T., and Letai, A. (2008). BIM and other BCL-2 family proteins exhibit cross-species conservation of function between zebrafish and mammals. Cell Death Differ. *15*, 1063–1072.

Jiao, J., Huang, X., Feit-Leithman, R.A., Neve, R.L., Snider, W., Dartt, D.A., and Chen, D.F. (2005). Bcl-2 enhances Ca(2+) signaling to support the intrinsic regenerative capacity of CNS axons. EMBO J. *24*, 1068–1078.

Koppen, M., Fernandez, B.G., Carvalho, L., Jacinto, A., and Heisenberg, C.P. (2006). Coordinated cell-shape changes control epithelial movement in zebrafish and Drosophila. Development *133*, 2671–2681.

Kowaltowski, A.J., and Fiskum, G. (2005). Redox mechanisms of cytoprotection by Bcl-2. Antioxid. Redox Signal. *7*, 508–514.

Lai, S.L., Chan, T.H., Lin, M.J., Huang, W.P., Lou, S.W., and Lee, S.J. (2008). Diaphanous-related formin 2 and profilin I are required for gastrulation cell movements. PLoS ONE *3*, e3439.

Lam, S.H., Wu, Y.L., Vega, V.B., Miller, L.D., Spitsbergen, J., Tong, Y., Zhan, H., Govindarajan, K.R., Lee, S., Mathavan, S., et al. (2006). Conservation of gene expression signatures between zebrafish and human liver tumors and tumor progression. Nat. Biotechnol. *24*, 73–75.

Lieschke, G.J., and Currie, P.D. (2007). Animal models of human disease: zebrafish swim into view. Nat. Rev. Genet. *8*, 353–367.

Link, V., Shevchenko, A., and Heisenberg, C.P. (2006). Proteomics of early zebrafish embryos. BMC Dev. Biol. *6*, 1.

Matsumura, F. (2005). Regulation of myosin II during cytokinesis in higher eukaryotes. Trends Cell Biol. *15*, 371–377.

Murphy, A.N., Bredesen, D.E., Cortopassi, G., Wang, E., and Fiskum, G. (1996). Bcl-2 potentiates the maximal calcium uptake capacity of neural cell mitochondria. Proc. Natl. Acad. Sci. USA *93*, 9893–9898.

Rizzuto, R., Marchi, S., Bonora, M., Aguiari, P., Bononi, A., De Stefani, D., Giorgi, C., Leo, S., Rimessi, A., Siviero, R., et al. (2009). Ca(2+) transfer from the ER to mitochondria: when, how and why. Biochim. Biophys. Acta *1787*, 1342–1351.

Rohde, L.A., and Heisenberg, C.P. (2007). Zebrafish gastrulation: cell movements, signals, and mechanisms. Int. Rev. Cytol. *261*, 159–192.

Rong, Y., and Distelhorst, C.W. (2008). Bcl-2 protein family members: versatile regulators of calcium signaling in cell survival and apoptosis. Annu. Rev. Physiol. *70*, 73–91.

Rong, Y.P., Bultynck, G., Aromolaran, A.S., Zhong, F., Parys, J.B., De Smedt, H., Mignery, G.A., Roderick, H.L., Bootman, M.D., and Distelhorst, C.W. (2009). The BH4 domain of Bcl-2 inhibits ER calcium release and apoptosis by binding the regulatory and coupling domain of the IP3 receptor. Proc. Natl. Acad. Sci. USA *106*, 14397–14402.

Shestopalov, I.A., and Chen, J.K. (2010). Oligonucleotide-based tools for studying zebrafish development. Zebrafish *7*, 31–40.

Shibasaki, F., Kondo, E., Akagi, T., and McKeon, F. (1997). Suppression of signalling through transcription factor NF-AT by interactions between calcineurin and Bcl-2. Nature *386*, 728–731.

Shirane, M., and Nakayama, K.I. (2003). Inherent calcineurin inhibitor FKBP38 targets Bcl-2 to mitochondria and inhibits apoptosis. Nat. Cell Biol. *5*, 28–37.

Solnica-Krezel, L. (2006). Gastrulation in zebrafish—all just about adhesion? Curr. Opin. Genet. Dev. *16*, 433–441.

Takashima, S. (2009). Phosphorylation of myosin regulatory light chain by myosin light chain kinase, and muscle contraction. Circ. J. *73*, 208–213.

Takayama, S., Sato, T., Krajewski, S., Kochel, K., Irie, S., Millan, J.A., and Reed, J.C. (1995). Cloning and functional analysis of BAG-1: a novel Bcl-2-binding protein with anti-cell death activity. Cell *80*, 279–284.

Totsukawa, G., Yamakita, Y., Yamashiro, S., Hartshorne, D.J., Sasaki, Y., and Matsumura, F. (2000). Distinct roles of ROCK (Rho-kinase) and MLCK in spatial regulation of MLC phosphorylation for assembly of stress fibers and focal adhesions in 3T3 fibroblasts. J. Cell Biol. *150*, 797–806.

Wang, C., and Youle, R.J. (2009). The role of mitochondria in apoptosis*. Annu. Rev. Genet. *43*, 95–118.

Wang, H.G., Miyashita, T., Takayama, S., Sato, T., Torigoe, T., Krajewski, S., Tanaka, S., Hovey, L., 3rd, Troppmair, J., Rapp, U.R., et al. (1994). Apoptosis regulation by interaction of Bcl-2 protein and Raf-1 kinase. Oncogene *9*, 2751–2756.

Wang, X., Belguise, K., Kersual, N., Kirsch, K.H., Mineva, N.D., Galtier, F., Chalbos, D., and Sonenshein, G.E. (2007). Oestrogen signalling inhibits invasive phenotype by repressing RelB and its target BCL2. Nat. Cell Biol. *9*, 470–478.

Webb, S.E., and Miller, A.L. (2006). Ca2+ signaling and early embryonic patterning during the blastula and gastrula periods of zebrafish and Xenopus development. Biochim. Biophys. Acta *1763*, 1192–1208.

Westfall, T.A., Hjertos, B., and Slusarski, D.C. (2003). Requirement for intracellular calcium modulation in zebrafish dorsal-ventral patterning. Dev. Biol. *259*, 380–391.

White, C., Li, C., Yang, J., Petrenko, N.B., Madesh, M., Thompson, C.B., and Foskett, J.K. (2005). The endoplasmic reticulum gateway to apoptosis by Bcl-X(L) modulation of the InsP3R. Nat. Cell Biol. *7*, 1021–1028.

Wilkins, S.J., Yoong, S., Verkade, H., Mizoguchi, T., Plowman, S.J., Hancock, J.F., Kikuchi, Y., Heath, J.K., and Perkins, A.C. (2008). Mtx2 directs zebrafish morphogenetic movements during epiboly by regulating microfilament formation. Dev. Biol. *314*, 12–22.

Youn, C.K., Cho, H.J., Kim, S.H., Kim, H.B., Kim, M.H., Chang, I.Y., Lee, J.S., Chung, M.H., Hahm, K.S., and You, H.J. (2005). Bcl-2 expression suppresses mismatch repair activity through inhibition of E2F transcriptional activity. Nat. Cell Biol. *7*, 137–147.

Zinkel, S., Gross, A., and Yang, E. (2006). BCL2 family in DNA damage and cell cycle control. Cell Death Differ. *13*, 1351–1359.